AD_____

Award Number: DAMD17-03-1-0342

TITLE: Elucidation of Prion Protein Conformational Changes Associated with Infectivity by Fluorescence Spectroscopy

PRINCIPAL INVESTIGATOR: Michele McGuirl, Ph.D.

CONTRACTING ORGANIZATION: The University of Montana
Missoula, MT 59812-1329

REPORT DATE: June 2006

TYPE OF REPORT: Annual

PREPARED FOR: U.S. Army Medical Research and Materiel Command
Fort Detrick, Maryland 21702-5012

REPORT DOCUMENTATION PAGE

Form Approved
OMB No. 0704-0188

1. REPORT DATE	2. REPORT TYPE	3. DATES COVERED
01-06-2006	Annual	15 May 2005 – 14 May 2006

4. TITLE AND SUBTITLE

Elucidation of Prion Protein Conformational Changes Associated with Infectivity by Fluorescence Spectroscopy

5a. CONTRACT NUMBER

5b. GRANT NUMBER
DAMD17-03-1-0342

5c. PROGRAM ELEMENT NUMBER

6. AUTHOR(S)

Michele McGuirl, Ph.D.

5d. PROJECT NUMBER

5e. TASK NUMBER

5f. WORK UNIT NUMBER

7. PERFORMING ORGANIZATION NAME(S) AND ADDRESS(ES)

The University of Montana
Missoula, MT 59812-1329

8. PERFORMING ORGANIZATION REPORT NUMBER

9. SPONSORING / MONITORING AGENCY NAME(S) AND ADDRESS(ES)
U.S. Army Medical Research and Materiel Command
Fort Detrick, Maryland 21702-5012

10. SPONSOR/MONITOR'S ACRONYM(S)

11. SPONSOR/MONITOR'S REPORT NUMBER(S)

12. DISTRIBUTION / AVAILABILITY STATEMENT
Approved for Public Release; Distribution Unlimited

13. SUPPLEMENTARY NOTES
Original contains colored plates: ALL DTIC reproductions will be in black and white.

14. ABSTRACT

Prion diseases are fatal neurodegenerative diseases of mammals. They are characterized by the conversion of normal prion protein (PrP) to a misfolded conformational state that accumulates as plaques in the brain. The diagnosis of prion diseases relies on the ability to differentiate between normal PrP and its misfolded, infectious form. This is difficult to accomplish by traditional testing methods, since it requires discerning between conformational states of a protein that is present in both normal and diseased tissue, rather than identifying the appearance of a new protein associated with infection. We wish to design a reporter PrP substrate that may be monitored by fluorescence spectroscopy. After the conversion of normal-PrP to its infectious state, some amino acid residues of PrP will undergo a change in their local solvent environment. We propose to identify these residues by monitoring the fluorescence emission spectrum of a series of mutant 7-AzaTrp-substituted PrP proteins. The 7-AzaTrp fluorescence emission spectrum is both unique compared with normal Trp and exquisitely sensitive to its local environment. This could lead to the development of a rapid, sensitive, and inexpensive technique to detect infectious PrP, based on its ability to bind 7-AzaTrp-substituted PrP, and convert it to the misfolded form.

15. SUBJECT TERMS
prion fluorescence assay structure 7-azatryptophan

16. SECURITY CLASSIFICATION OF:				18. NUMBER OF PAGES	19a. NAME OF RESPONSIBLE PERSON
					USAMRMC
a. REPORT	b. ABSTRACT	c. THIS PAGE			19b. TELEPHONE NUMBER *(include area code)*
U	U	U	UU	31	

Standard Form 298 (Rev. 8-98)
Prescribed by ANSI Std. Z39.18

Table of Contents

INTRODUCTION

Prion diseases are fatal neurodegenerative diseases of mammals and include Creutzfeld-Jacob disease (humans), scrapie (sheep), chronic wasting disease (elk, deer), and mad cow disease (cattle).(1) The diseases are characterized by the conversion of normal prion protein (PrP) to a misfolded conformational state that aggregates and forms plaques in the brain. Although this conversion process is poorly understood, it is known that the aggregate-prone form has a higher β-sheet content than does normal PrP. To differentiate between normal PrP and its misfolded, infectious form and assist in diagnosis of the diseased state, we wish to design a reporter PrP substrate peptide that will exhibit unique fluorescent properties upon contact with infectious PrP and/or its subsequent conversion. The sequence of the reporter peptide will be based upon experiments conducted with recombinant PrP. We will identify individual PrP residues that undergo changes in their local solvent environment upon conversion by measuring the fluorescence emission spectra of a series of mutant 7-AzaTrp-substituted PrP proteins. The 7-AzaTrp absorbance spectrum is red-shifted compared with Trp, and its fluorescence emission spectrum is exquisitely sensitive to its local environment.(2) Therefore, the conversion of the analog-substituted PrP substrate will be easily detected against a background of Trp-containing protein aggregates.

BODY

Overview

In this past year we have finished *Task 1* and have made some progress on *Task 2.* We have asked for, and received, an no-cost extension so that the work may be completed. (As such, this is not actually the "final" report and is written as a third "annual" report.)The extension was necessitated by continued difficulties in training personnel. The student who was being trained during year 2, Ms. Yanchao Ran, was unable to meet the academic requirements of the program and left the university. Dr. Rong Wang finished his limited work on copper binding to several of the Trp mutants (*Task 1e*) before starting his postdoctoral studies at Rocky Mountain Laboratories/NIAID. A new graduate student, Mr. Chris Lennon, along with Dr. Holly Cox, a short-term hire at the post-doctoral level, began using a new technique to help define regions of difference between α- and β-forms of PrP. These have resulted in an article that was recently submitted to *Biochemistry.* To better understand our results, we have entered into a computational study in collaboration with Dr. Patrik Callis, an expert in the theoretical understanding of Trp fluorescence in proteins. We anticipate being able to publish the fluorescence data shortly. Ms. Jessica Gilbert is a new graduate student who is continuing to work on this project. Dr. Scott Hennelly also worked part-time on the project this year, to facilitate the transfer of knowledge and technique development.

Accomplishments related to Task 1. **Identify surface residues of the normal PrP form that change conformation and/or participate in binding to aggregated PrP. (Months 1-24)**

1a) Express a series of Trp-substituted mutants of truncated Syrian hamster PrP (90-231) in E. coli.

Expression: We have expressed truncated Syrian golden hamster PrP (residues 90-231) in *E. coli*, as outlined in the Methods Section of our proposal. We continue to use the robust pET expression vector and the Rosetta cell strain (Novagen) for expression, since it is proven to work for full-length PrP. (5) By using the commercially available Rosetta cell strain from Novagen, we have increased the expression levels of both full-length and truncated PrP to nearly 30 mg/liter of culture.

Mutants Produced: This year finished making all the desired priority mutants that were summarized in Table 1 of the previous report (11 total).
Purification: We have purified all eleven mutants to homogeneity using the protocol outlined in the previous report. Typical yields are 10 mg purified PrP per liter of culture. One mutant in particular, G123W, was obtained only in low yields.

Tasks 1 (b-d) For each mutant: (b) determine the stability of the α-structure by CD (circular dichroism) temperature unfolding experiments; (c) determine the solvent exposure of the introduced Trp residue by fluorescence spectroscopy; and (d) determine if conversion to a soluble β-structure changes the solvent exposure by fluorescence spectroscopy.

This has been done for each of the 10 Trp-containing mutants (in duplicate), as previously described. All mutants were stable below 55C. The fluorescence results are summarized in Table 1 and represent data normalized to 20 μM protein.

Protein	λ_{max} shift (α-→ β) (nm)	Intensity change (%)	α-PrP (λ max, Signal Intensity)		β-PrP (λ max, Signal Intensity)	
W99 (W145Y)	-2	+12	352	0.100	350	0.112
G123W (W99F/W145Y)	-5	-2	353	0.276	348	0.272
L125W (W99F/W145Y)	-5	+25	351	0.143	346	0.18
S135W (W99F/W145Y)	-10	-45	354	0.416	344	0.221
D144W (W99F/W145Y)	-9	-23	354	0.228	345	0.174
W145 (W99F)	-3	+33	352	0.201	349	0.268
Y150W (W99F/W145Y)	+8	-71	381	0.100	389	0.028
N159W (W99F/W145Y)	-8	-40	352	0.471	344	0.280
Y163W (W99F/W145Y)	+10	+295	335	0.071	345	0.21
Y218W (W99F/W145Y)	+13	+295	334	0.049	347	0.146

Table 1. Mutants of PrP prepared in this study.

The data indicate that Y163W and Y218W may be the best reported positions of β-PrP, since they undergo large intensity increases and red-shifts. We will continue to work on understanding the fundamental properties of these mutants as we move toward developing the reporter peptide in *Task 2.*

The availability of the coordinates for two distinct models for β-PrP makes it possible to do detailed computational analyses of the Trp fluorescence data. This will be done with the guidance of Dr. Patrik Callis from Montana State University/Bozeman. Dr. Callis is a world-renowned expert in the theory and computational analysis of Trp fluorescence. (11,12) We plan to interpret the fluorescence spectra of α-PrP in relation with its NMR structure, and to then do the same for the two β-PrP models. This was not accomplished in the previous year because Dr. Callis did not have anyone available to work on the project. This is no longer a problem. Preliminary analysis of the data in Table 1 lead us to believe that neither model can account for the sum of the observed Trp fluorescence behaviors of the β-PrP mutants we produced. Whereas one model better fits the data generated from one mutant, the other model better fits the data from a different mutant. Hence, we believe that neither model is likely to be "correct" and that the true structure of β-PrP must be different from either model.

We have followed the kinetics of conversion of Y150W and wild type PrP to the β-PrP state by Asymmetric Flow Field Flow Fractionation (AF_4) and ANS fluorescence (Figure 1). ANS monitors the formation of β-PrP by changing the fluorescence of the ANS dye, while AF_4 montiors changes in aggregate size. The Y150W protein converted twice as fast as the wild type protein (both techniques gave the same results). Analysis of the aggregate size using the MALS detector suggests that the β-form is best described as an octamer. We plan to check the kinetics of other mutants in the future, especially the reportere protein designed in *Task 2*.

Figure 1. AF_4 trace of the conversion of wild type PrP.
Inset: conversion monitored by ANS binding

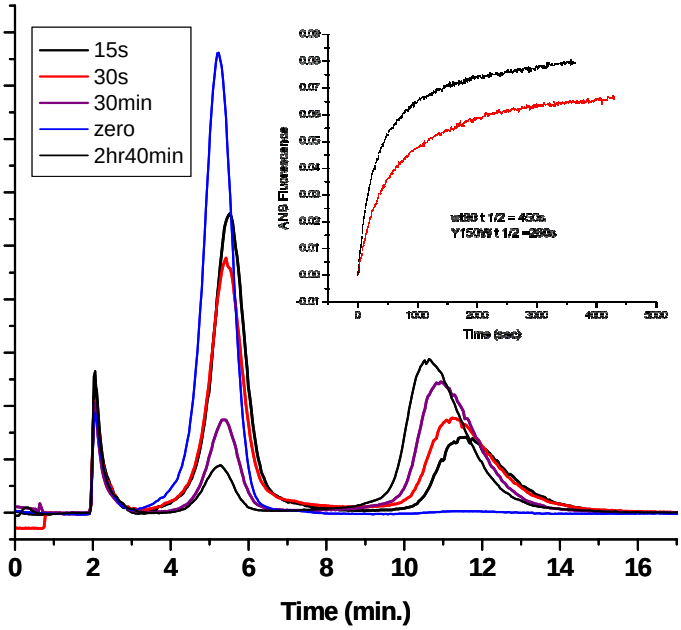

Task 1e. For each mutant, determine if copper or manganese binding influences fluorescent spectrum of either the soluble α-form or soluble β-form.

We have found that copper(II) does indeed influence the fluorescence spectrum of the Trp mutants, but in a non-specific way. Copper(II) is reported to bind to residues 90-119, interacting and ligating specifically with His96 and possibly His111.

Table 2. Measured Kd values of Cu(II)

Sample	Kd app (μM) 50 mM MOPS, pH 8.5	Kd app (μM) 0.1 M Tris, pH 8.5
Wild type	140	571
W99 only	90	461
W145 only	148	nd
L125W only	195	751
NATA (tryptophan)	nd	670

When we measured the Trp fluorescence of the ild type protein, we found that Cu(II) did indeed quench the Trp fluorescence signal (Table 2 and Figure 2). The observed Kd was buffer-dependent, with more copper being required to quench the signal when a metal chelating buffer such as Tris was used. We then began to investigate the *specificity* of the quenching, by testing different Trp mutants. If the quenching is caused by copper binding at the His96 site, then we reasoned that W99 might show a strong quenching whereas W145 would not. To our surprise, this was not the case. We then tested the L125W mutant. Again, we anticipated that we would observe very different observed Kd values, since L125W and W145 are on opposite faces of the α-PrP structure. Although the copper site at His96 is in the dynamically floppy N-terminus, it cannot "reach around" to the L125W site, whereas it can readily access W145 and W99. To our surprise, the Kd values of the L125 mutant were similar to other mutants. Indeed, when we tested N-acetyltryptophanamide, we found that is is similarly quenched by Cu(II). We interpret this to mean that the quenching is due to excess copper interacting with the protein in general and is not due to the specific binding of copper at His96. Thises findings are significant for two reasons: (1) they refute published data that claim evidence of a high affinity copper binding site at His99, as determined by the quenching of Trp fluorescence in the multi-Trp, full-length protein; and (2) the very high concentrations of copper required to quench the Trp fluorescence of PrP are non-physiological and will not interfere with the fluorescence of any reporter protein we use in *Task 2.*

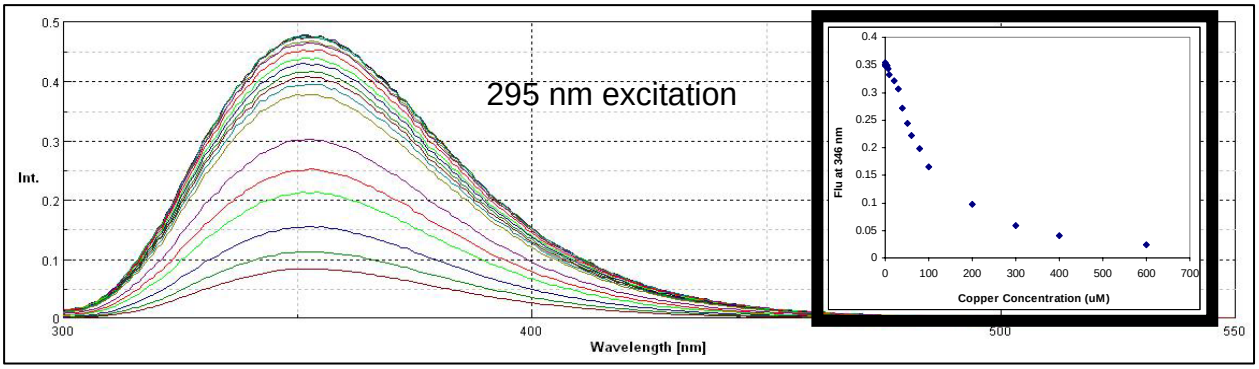

Figure 2. Quenching of Trp Fluorescence by Cu(II).

In our quest to better understand the differences between the α and β forms of PrP, we chose to do additional biophysical studies. We used two nitration agents, peroxynitrite and tetranitromethane, to probe the isoforms for structural differences. These reagents chemically modify Tyr residues. We discovered that Tyr149 and Tyr150 are reactive only in the β-form, whereas Tyr 162 and Tyr 163 were somewhat reactive in both. Tyr218 was much less reactive in the β-form. Like Trp fluorescence, susceptibility to nitration is dictated by many factors other than solvent exposure. However, the combined results suggest that we should pursue Y150W, Y163W and Y218W for Task 2 studies. The nitration experiments have been submitted to *Biochemistry* – see attached manuscript.

Accomplishments related to Task 2. **Create a 7-AzaTrp-substituted PrP protein as a reporter protein that may be used to detect infectious PrP in the field. The fluorescence spectrum of this substrate protein will be determined in its soluble α- and β-forms. The substrate protein will be exposed to an aggregated, insoluble β-form of PrP (PrP-res) produced by *in vitro* techniques. This will mimic the conversion of the substrate protein by infectious PrP. The overall yield and time course of conformational changes in the substrate protein will be determined by monitoring changes in the 7-azatryptophan fluorescence. (Months 25-36)**

We have chosen to focus on three mutants for this study, as the newly introduced mutants that were added to the mutant list (Table 1) did not show any more advantageous behavior. Of the mutants, Y163W shows the greatest increase in fluoresecence intensity upon conversion to the β-form (see prior report), but the nitration data suggests that all three should be examined. Recently we have begun making fibrils of recombinant PrP, with the advice of Dr. Roger Moore from Rocky Mountain Labs. We are now in a position to assess if large changes in fluorescence will also occur upon conversion of these three mutants to the fibrillar form. This will provide the basis for completing this task. If the fibrillar forms of the AzaTrp-subsituted mutants show the anticipated changes, we will conclude the study by measuring the changes that occur when a seed of normal protein is used to fibrillize the best of the three AzaTrp mutant reporter proteins.

KEY RESEARCH ACCOMPLISHMENTS

- Produced, purified, and characterized eleven mutants of Syrian hamster prion protein
- Measured the fluorescence emission spectra of these mutants in their normal monomeric α-form
- Determined the fluorescence emission spectra of the mutants after conversion to the β-form
- Determined that Y150W, Y163W, and Y218W are the three candidates for reporting structural changes that accompany conversion
- Submitted a paper to *Biochemistry*

REPORTABLE OUTCOMES:

The first YYR motif and the C-terminus of PrP undergo structural changes upon conversion to the β-form of PrP. See Probing Structral Differences in Prion Protein Isoforms by Tyrosine Nitration. CW Lennon, HD Cox, SP Hennelly, SJ Chelmo, and MA McGuirl; *submitted to Biochemistry Augist 2006*

CONCLUSIONS:

We have made substantial progress toward determining key residues of the prion protein that undergo structural perturbations upon conversion to the disease-causing conformation. We have identified several positions that report on the structural changes associated with conversion. We have improved our productivity by purchaseing an M2e microplate reader with fluorescence capabilities. This will streamline the time needed to complete the measurements and allow us to assay fibrils by fluorescence.

REFERENCES:

1. B. Caughey *et al.*, *Adv Protein Chem* **57**, 139 (2001).
2. J. B. Ross, A. G. Szabo, C. W. Hogue, *Methods Enzymol* **278**, 151 (1997).

MANUSCRIPTS/REPRINTS, ABSTRACTS

Probing Structral Differences in Prion Protein Isoforms by Tyrosine Nitration. CW Lennon, HD Cox, SP Hennelly, SJ Chelmo, and MA McGuirl; *submitted to Biochemistry August 2006*

APPENDICES

Probing Structral Differences in Prion Protein Isoforms by Tyrosine Nitration. CW Lennon, HD Cox, SP Hennelly, SJ Chelmo, and MA McGuirl; *submitted to Biochemistry August 2006*

Title: *Probing Structural Differences in Prion Protein Isoforms by Tyrosine Nitration*[†]

[†]This work was supported by grants to MAM from the US Army Research (DAMD17-03-1-0342) and the NIH COBRE program (P20 RR020185-01).

Authors: Christopher W. Lennon,[‡,⊥] Holly D. Cox,[§,⊥] Scott P. Hennelly,[‡] Sam J. Chelmo,[‖] and Michele A. McGuirl*[,‡]

[‡] Division of Biological Sciences and the Biomolecular Structure and Dynamics Program, The University of Montana, Missoula, MT 59812 USA

[§] current address: Department of Pathology, the University of Utah, 50 N. Medical Dr. Salt Lake City, UT 84132

[‖] current address: Sanford School of Medicine, the University of South Dakota, 1400 West 22nd St, Sioux Falls, SD 57105

* corresponding author

⊥ contributed equally to this work

Corresponding author information:
Michele A. McGuirl
Clapp Building 204, Division of Biological Sciences
32 Campus Drive The University of Montana
Missoula, MT 59812
michele.mcguirl@umontana.edu
(406) 243-4404 phone
(406) 243-4304 fax

Running Title: *Probing Prion Isoforms by Tyrosine Nitration*

Abbreviations:
AF_4, asymmetric flow field flow fractionation; CD, Circular Dichroism; ESI, Electrospray ionization; GPI, glycosylphosphatidylinositol; MAb, monoclonal antibody; MALDI, matrix assisted laser desorption ionization; MRE, mean residue ellipticity; MS, mass spectrometry; MS/MS tandem mass spectrometry; NMR, nuclear magnetic resonance; PN, peroxynitrite; PrP, prion protein; PrP90, residues 90-232 of hamster prion protein; PrP^C, cellular prion; PrP^{Sc}, scrapie prion; TCA, trichloroacetic acid; TFA, trifluoroacetic acid; TNM, tetranitromethane; TOF, time of flight.

Abstract

Two conformational isomers of recombinant hamster prion protein (residues 90-232) have been probed by reaction with two tyrosine nitration reagents, peroxynitrite and tetranitromethane. Two conserved tyrosine residues (tyrosines 149 and 150) are not labeled by either reagent in the normal cellular form of the prion protein. These residues become reactive after the protein has been converted to the β-oligomeric isoform, which is a model of the fibrillar form that causes disease. After conversion, a decrease in reactivity is noted for two other conserved residues, tyrosine 225 and tyrosine 226, whereas little to no effect was observed for other tyrosines. Thus, tyrosine nitration has identified two specific regions of the normal prion protein isoform that undergo a conformational change upon conversion.

Introduction

Prion diseases are a class of fatal neurodegenerative disorders (*1, 2*) that include Creutzfeldt-Jakob disease, Gerstmann-Sträussler-Scheinker syndrome, kuru and fatal familial insomnia in humans, bovine spongiform encephalopathy (mad cow) in cows, chronic wasting in deer and elk, and scrapie in sheep. Prion diseases belong to the larger category of amyloidoses that also includes Alzheimer's, Parkinson's, Huntington's and Amylotrophic Lateral Sclerosis diseases. The common characteristic of amyloid diseases are the formation of ordered aggregates of misfolded proteins in the brain, which are associated with plaque deposits and neurodegeneration (*3*). Each type of amyloidosis is associated with a specific misfolded protein; prion diseases involve the prion protein (PrP). However, prion diseases are also unique among amyloidoses in that they are transmissible, in addition to being inherited or sporadic (*2, 4*).

Unlike other infectious agents, prions do not require a nucleic acid component, i.e., DNA or RNA, for infection to occur. Indeed, the name “prion” is derived from the blending of the first two syllables of the term “proteinaceous infectious" particle (*5*). According to the "protein only" hypothesis of prion replication, an infectious, misfolded oligomeric PrP particle causes the normal, non-infectious monomeric cellular form of PrP, called PrP^{C}, to undergo a conformational change. This conversion event leads to the incorporation of normal PrP monomers into the infectious aggregated particle, ultimately leading to the formation of fibrils. The fibrillar form of PrP is known as PrP^{Sc}, since it was first associated with scrapie. No covalent modifications are known to occur during or after the conversion process; the difference between PrP^{C} and PrP^{Sc} is purely conformational (*6, 7*).

Syrian hamster PrP is an extracellular neuronal protein that is made from a 254-amino acid residue precursor protein. Residues 1-22 comprise the signal peptide that is cleaved upon translocation. Residues 233-254 signal for the addition of a glycosylphosphatidylinisotol (GPI) lipid anchor at residue 232, which holds PrP in the membrane. These residues are also cleaved during processing. Mature PrP has the ability to form several distinct and stable isoforms. PrP^{C} is the normal cellular

conformation, for which many high resolution structures from numerous mammalian sources have been determined by both nuclear magnetic resonance (NMR) (*8-15*) and X-ray crystallography (*16-18*). PrP^C is a soluble monomer dominated by an α-helical C-terminal domain (residues 125-232) and a large unstructured N-terminus (residues 23-89) (*19*). PrP^{Sc} is the pathological conformer that is enriched in β-sheet secondary structure and which forms insoluble fibrils (*20, 21*).

Another isoform that is enriched in β-sheet structure is the β-oligomer. This is a spherical aggregate (8-12 subunits) produced in vitro, usually from recombinant PrP^C protein that lacks the GPI anchor. The β-oligomer shares many physical characteristics with PrP^{Sc} (*22-26*) including its toxicity to cultured cells (*27*), yet it remains soluble. For these reasons, the β-oligomer is widely viewed as a useful and more tractable model for PrP^{Sc}. This is further supported by an intriguing discovery made by Caughey and coworkers in their search to determine the size of the smallest infectious prion aggregate [(28)]. Particles made from the chemical disruption of PrP^{Sc} fibrils, which were of similar size and shape as β-oligomers, were found to be more infectious than the large fibrils, per protein subunit. Furthermore, conditions necessary for the formation of the β-oligomeric form of recombinant PrP have been shown to promote their conversion to well ordered fibrils upon extended incubation (*22, 23*).

The insoluble and fibrillar nature of infectious PrP^{Sc} has hampered the elucidation of its structure at the molecular level, in stark contrast with the wealth of data available for PrP^C. However, many gross structural characteristics of PrP^{Sc} have been determined. Treatment with the non-specific protease proteinase K showed that while PrP^C is sensitive to proteolysis, PrP^{Sc} fibrils can form a resistant core consisting of amino acid residues ~90-232 (*29*). Mutagenesis studies of the unstructured N-terminal region of PrP (residues 23-89) indicate that it is not required for infectivity or fibril formation (*30-33*), although it does influence these properties (*34-36*). Fourier Transform Infrared spectroscopy, which measures the frequencies arising from the stretching vibrations of peptide carbonyl groups, has indicated that the transition from PrP^C to PrP^{Sc} is associated with a small loss in α-helicity and a large increase in β-sheet secondary structure (*6, 37*). This was confirmed using Circular Dichroism (CD) spectroscopy (*4*), which measures protein secondary structure. Similar structural changes are observed when recombinant PrP^C is converted to the β-oligomer state or to the fibrillar form, when either full-length PrP (residues 90-232) or the truncated version (residues 90-232, often designated PrP90) is used (*23, 24*) . The ultrastructure of PrP^{Sc} has also been probed using low-resolution crystallography (*38, 39*), and several microscopy studies have been conducted with recombinant PrP fibrils (*23, 40*). Multiple research groups have combined the available biophysical data with computational techniques to generate models for PrP^{Sc} (*38, 39, 41-45*) . Although these models differ significantly in the details of the proposed PrP^{Sc} subunit structures, each includes intersubunit contacts formed by β-strand interactions as the basis for fibril formation.

Some molecular details of PrP^{Sc} are also beginning to emerge. Antibody studies have identified selective epitopes in the C-terminal half of PrP that are surface accessible in PrP^{Sc} but not in PrP^{C} (*46-49*). One of these epitopes is a Tyr-Tyr-Arg (YYR) motif, of which there are two in the primary structure (*46*). Cashman and coworkers favor assignment of the second YYR motif (residues 162-164) as the antigenic site (*46*). They also noted changes in tyrosine fluorescence that were consistent with the solvent exposure of at least some Tyr residues upon conversion of PrP^{C} to the infectious state. Since solvent-exposed tyrosyl residues are often more susceptible to chemical nitration than buried residues (*50*), we hypothesized that more of the ten Tyr residues present in hamster PrP90 would react with nitrating reagents in the β-oligomeric state, which is structurally similar to PrP^{Sc}. We tested this by reacting recombinant truncated hamster PrP90 (residues 90-232 containing 10 tyrosyl residues) in its PrP^{C} and β-oligomer isoforms with two nitrating reagents, peroxynitrite (PN) and tetranitromethane (TNM). Nitration efficiency was then assessed by peptide mapping via mass spectrometry (MS) (*50, 51*). As anticipated, conformationally-dependent labeling patterns were detected. We have identified two specific regions of PrP^{C} that undergo a conformational change upon conversion. In sharp contrast to the results predicted from antibody studies (*46*), only the first YYR motif (residues 149-151) is selectively nitrated in the β-oligomeric state.

Experimental Procedures

Production of recombinant PrP90 Isoforms

The codons for residues 90-232 of Syrian hamster prion protein were sub-cloned from plasmid pHaPrP (*52*) into $pET24a^{+}$, creating the expression plasmid pET24PrP90. This construct produces a truncated recombinant protein (PrP90) in which most of the unstructured N-terminal domain has been omitted, along with the C-terminal residues associated with the mammalian GPI anchor. High levels of expression (> 15 mg/L) were achieved in *E. coli* BL21(DE3)-Rosetta cells (Novagen, Inc). Typically, three liters of liquid culture were grown at 37°C to an OD_{600} of 1.0 in 2xYT(*53*) media supplemented with 50 µg/mL kanamycin and 34 µg/mL chloramphenicol. Expression of PrP90 was then induced with 0.5 mM isopropyl-β-D-thiogalactoside. Cells were harvested four hours post-induction and frozen overnight.

PrP90 was purified using modifications to a published procedure (*52*). Frozen cells were suspended in lysis buffer (50 mM TrisCl, pH 7.5 containing 100 µg/mL lysozyme and 10 µg/mL DNase I) for 1.5 hours at 37°C with shaking. Inclusion bodies were purified from the lysis pellet by repeated incubation in 50 mM Tris-Cl, pH 7.5 containing 1% Triton X-100 followed by centrifugation. They were then solubilized in Buffer A (0.1 M KPO_4, 8 M urea, pH 8.0) containing protease inhibitor cocktail (Sigma). After centrifugation, the solublized, unfolded protein was batch-bound to 50 mL Ni(II)-Chelating Sepharose resin (GE Healthcare), which was then poured into a 5-cm diameter column and washed with Buffer A until the A_{280} of the eluent dropped below 0.3. PrP90 was refolded on the column by applying a 2-liter linear gradient from Buffer A to Buffer B (0.1 M KPO_4, pH 8.0), followed by washing

with several column volumes of Buffer B. PrP^C was eluted with Buffer B containing 60 mM imidazole. When necessary, further purification was accomplished using Hydrophobic Interaction Chromatography. Briefly, ~10 mg of PrP90 was loaded onto a HiPrep Phenyl Sepharose 16/10 column (GE Healthcare) in 10 mM KPO_4, 6 M Guanidine-HCl, 1 M NH_4SO_4, pH 8, and eluted with a NH_4SO_4 gradient from 1.0 to 0 M in 25 mM TrisCl, pH 8.0 containing 4 M urea. The sample was then extensively dialyzed into 10 mM ammonium acetate buffer, pH 7. The protein was then used for experiments or lyophilized and stored at -20°C.

To form the β-oligomer, the lyophilized PrP^C pellet was first re-suspended and unfolded in 10 mM KPO_4, 6M Guanidine-HCl, pH 8 to a final concentration of 120 µM protein. This was then diluted six-fold with conversion buffer (60 mM sodium acetate, 160 mM NaCl, 3.6 M urea, pH 3.7) and incubated at 37°C overnight. Next, the samples were dialyzed into a suitable nitration reaction buffer.

Protein purity was assessed by SDS/PAGE analysis, performed on a Pharmacia PhastSystem (GE Healthcare) using 8-25% polyacrylamide gels and Coomassie Blue staining, according to the standard protocols suggested by the manufacturer. Bio-Rad Broad Range Molecular Weight Marker was used as a standard. Circular Dichroism (CD) spectra were measured on a Jasco 810 spectrophotometer equipped with a peltier temperature controller. Conversion was also followed by asymmetric flow field flow fractionation (AF_4) on an AF2000 instrument (PostNova, Inc), equipped with in-line UV-Vis and 7-angle multi-angle light scattering detectors. Samples of 400 pmoles or more were injected and focused for 35 s with a cross flow of 2 ml/min and a channel flow of 1 ml/min in 25 mM sodium acetate buffer containing 3 M urea, pH 5.0. Peaks were resolved using a 3 ml/min cross flow and a channel flow of 1 ml/min. The concentrations of purified PrP^C samples were determined using the theoretical extinction coefficient (*54*) at 280 nm of 26,025 $M^{-1}cm^{-1}$. After conversion to the β-oligomer and/or nitration, protein concentration was determined with the Bio-Rad Protein Dye Assay Kit, using untreated PrP^C as the protein standard.

Nitration of PrP Isoforms

All nitration reactions were performed at room temperature and all experiments were conducted in triplicate. Peroxynitrite (PN) was prepared according to a published procedure (*55*) with the following modification and stored at -70°C prior to use: a Bio-Logic SFM400 four-syringe quench flow apparatus was used to mix the components, to maximize the yield of potassium peroxynitrite. PN reactions were performed in 200 mM sodium acetate buffer, pH 5.5, containing 10 µM diethylenetriaminepentaacetic acid, whereas 50 mM sodium acetate buffer, pH 5.5 was used for tetranitromethane (TNM) reaction. The protein concentrations in all samples were ~12 µM. Samples were vortexed during the addition of PN and the protein-PN mixture was allowed to react for 5 minutes prior to cleanup. TNM was added to protein under anaerobic conditions and the reaction was allowed to proceed overnight for PrP^c or 2 hours for the β-oligomer.

After nitration, reaction side products were removed by dialysis and the protein was concentrated by precipitation with trichloroacetic acid (TCA). Protein pellets (~15 μg) were resuspended in 50 mM ammonium bicarbonate buffer, pH 8 containing trypsin at a ratio of 1:7.5 and digested at 37°C overnight. Tryptic peptides were reduced in 10 mM dithiothreitol for 1 hour at 56°C and the solution was dried under vacuum. Peptides were re-suspended in 50% acetonitrile and 0.1% trifluoroacetic acid (TFA), mixed 1:1 with α-cyano-4-hydroxycinnamic acid matrix spiked with a 1:8 dilution of Bruker Peptide Standards for internal calibration. Peptide mass spectra were acquired using a MALDI (matrix assisted laser desorption ionization) –TOF (time of flight) mass spectrometer (ABI Voyager DE Pro). The level of nitration for each tyrosine-containing peptide was estimated by taking the sum of the peak area for each m/z assigned to the nitrated peptide (+45), the deoxy-nitrated peptide (+29) and the dideoxy-nitrated peptide (+13) and dividing by the total peak area from the modified and unmodified tyrsoine-containing-peptide. This method accounts for the characteristic loss of one and two oxygens from the nitroTyr group, caused by photodecomposition associated with the UV wavelength of the MALDI laser (*56*). Tyrosine-containing peptides with methionine oxidation, with and without nitration, were also included in the quantification. Additional potential side-products associated with protein nitration were not encountered. For intact protein mass analysis, PrP^c was concentrated by TCA precipitation and the protein pellet was resuspended in 50% acetonitrile, 0.1% TFA at a concentration of 1 μg/μl. The protein was mixed 1:1 with a saturated solution of sinapinic acid matrix and analyzed in linear mode. External calibration was performed using Bruker protein standards II.

To confirm the site of nitration on tryptic peptides containing more than one tyrosine, sequence information was obtained by electrospray ionization (ESI) tandem mass spectrometry (MS/MS) analysis using a QTOF micro (Waters, Milford, MA). For sequence analysis of the YYR-peptide 149-151, cyanogen bromide digestion was performed on TCA precipitated protein pellets (15 μg) in 70% TFA at room temperature for 24 hours and the digestion solution was removed under vacuum. Peptides from both trypsin and cyanogen bromide digestion were resuspended in 2% acetonitrile, 0.1% formic acid and separated by capillary liquid chromatography using a CapLC XE (Waters) coupled to the ESI source of the QTOF micro. The peptides were concentrated and desalted with an in-line C_{18} PepMap™ Nano-Precolumn, 5 mm x 300 μm, 5 μm particle size (Dionex) followed by reversed phase separation on a Waters C_{18} capillary column (15 cm x 75 μm i.d., 3 μm particle size). Peptides were eluted from the column with a 70-minute linear gradient of acetonitrile from 10-40% in 0.1% formic acid. The voltages were set at 3800 V for the capillary, 38 V for the sample cone and 3.0 V for the extraction cone. Mass spectra were acquired between the range of 200-1500 m/z followed by data-dependent selection of ions for ms/ms. To enhance the selection of low abundance nitropeptides for MS/MS, only ions with m/z values that corresponded to nitropeptide masses with a 2+ or 3+ charge state were selected for collision induced dissociation fragmentation. Ions with m/z values corresponding to the unmodified peptides were not selected for ms/ms. Collision voltages were dependent upon the m/z and charge state of the parent ion. MS/MS spectra were analyzed using Mascot Daemon (Matrix Science) to search a

database containing the hamster PrP90 sequence. Methionine oxidation and nitro-tyrosine were selected as variable modifications. Mass accuracy was set to 50 ppm for peptide tolerance and 0.2 Da for MS/MS tolerance. Solvent exposure was determined using MOLMOL software (*57*).

Results

Protein Purification and Characterization

Using the BL21(DE3)-Rosetta/pET24PrP90 expression system, over 10 mg of PrP^C was routinely obtained per liter of culture, at a purity level of over 95%. The protein is produced as inclusion bodies that are readily purified from the cell paste. Refolding of the protein on the Ni(II)-chelating column leads to the formation of PrP^C, which may be converted to its β-rich conformational isomer. The Circular Dichroism (CD) spectra of the PrP^C and β-oligomeric forms of PrP90 are displayed in Figure 1. The high α-helical content of the PrP^C conformer is evident by both the overall shape (two negative peaks at 209 and 222 nm) and by the large Mean Residue Ellipticity (MRE) value (-13,000 ± 1000 deg-cm^2 dmol^{-1} residue^{-1}) at 222 nm. After conversion, the CD spectrum takes on the characteristics of a β-sheet protein, with a single negative peak centered at 214 nm and a smaller MRE value of -7,500 ± 500 deg-cm^2 dmol^{-1} residue^{-1}. Analysis of the two isoforms by asymmetric flow field flow fractionation (AF_4) using in-line UV (Figure 1, inset) and dynamic light scattering detection confirms that PrP^C is a monomeric species and that the β-oligomer is an octamer. This is consistent with published reports that the β-oligomeric form of both PrP90 and the full-length recombinant protein (residues 23-232) contains 8-12 PrP subunits (*22, 24, 58, 59*). Conversion to the β-oligomer is efficient, with only ~ 5 – 10 % remaining in the PrP^C state after overnight reaction. This fraction was readily removed from the β-oligomer by AF_4 separation. Re-injection of the purified β-oligomer peak did not show any significant re-formation of PrP^C (data not shown), even after several days storage.

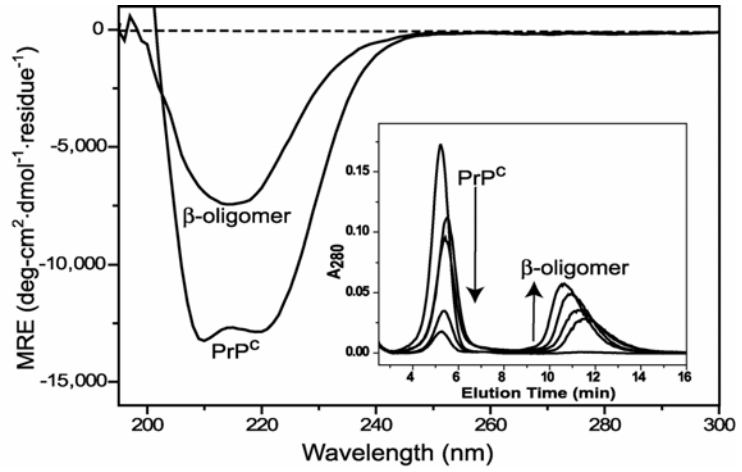

Figure 1. CD spectra of PrP conformational isomers. Inset: the AF_4 elution profiles (detection at 280 nm) showing the time course of the chemical conversion of PrP^c to the β-oligomer. Times of conversion: t = 0, 15s,

MALDI-TOF mass spectrometry of the intact protein indicates that the N-terminal methionine encoded by the vector is processed by the *E. coli* host (theoretical mass with N-terminal Met, 16462.2 Da; without N-terminal Met, 16,331.1 Da; experimental mass 16,329 ± 2 Da). This N-terminal processing is expected for cytosolic proteins

when the side chain of the penultimate amino acid, in this case Gly90 of PrP, is small (*60*). MALDI-TOF analysis of a tryptic digest of the recombinant protein indicates that the disulfide bond between the two existing Cys residues, Cys179 and Cys214, is also intact. This results in the presence of a peak with the average mass of 3732.42 Da detected in linear mode that disappears upon peptide treatment with 10 mM dithiothreitol.

Reaction of PrP90 Isoforms by Peroxynitrite and Tetranitromethane

Initial nitration experiments used a wide range of nitrating reagent concentrations. However, when PrP^C is reacted with PN at concentrations ≥ 150-fold over protein (15-fold over Tyr residues), AF_4 analysis showed the presence of higher molecular weight species in these samples (Figure 2A). Furthermore, the CD spectra indicate a significant loss in α-helicity (Figure 2A, inset). The higher ordered aggregates persisted even in an SDS/PAGE gel (Figure 3), indicating that the newly formed aggregates represent covalently crosslinked subunits. Similar results were obtained when the β-oligomer was labeled with 250x PN or TNM (Figures 2B and 3). Thus, subsequent experiments were restricted to treatment with 100x nitrating reagents (10-fold excess over Tyr residues) for the β-oligomer and 100x PN for PrP^C, and the structural integrity of each sample was verified after treatment by CD and AF_4 analysis. Under these conditions, PN effectively labeled both PrP^C and the β-oligomer, whereas TNM reacted well with the β-oligomer but poorly with PrP^C (Table 1).

Figure 2. AF_4 elution profiles of the PrP isoforms treated with increasing concentrations of PN. (——) untreated control, (**-----**) 100x PN reaction, (·····) 250x PN reaction. (**A**) the PrP^C isoform, with the corresponding CD spectra presented (inset). (**B**) the β-oligomer.

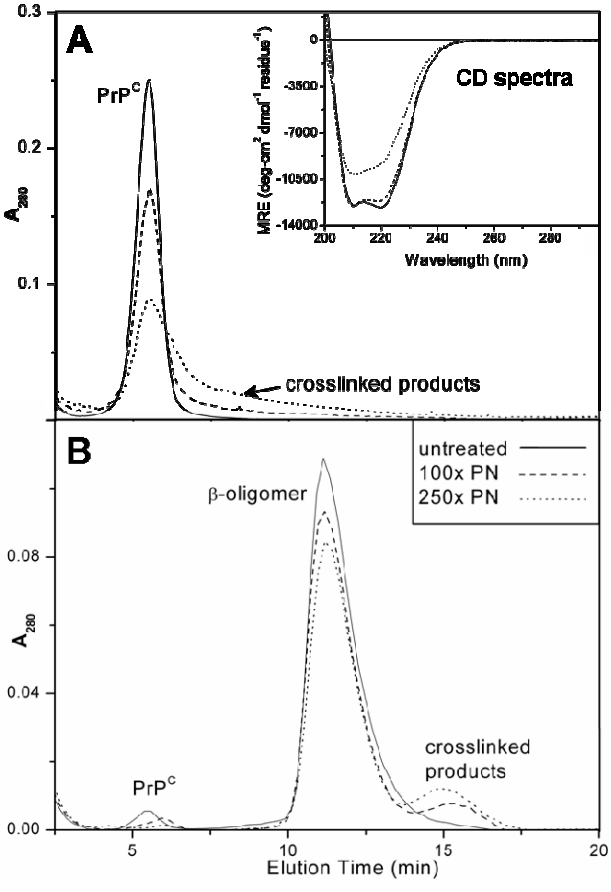

Figure 3. SDS/PAGE analysis of PN and TNM reactions with PrP^C and the β-oligomer. Lane S, MW standard;. Lane 1, PrP^c untreated control; Lane 2, PrP^c + 250x PN; Lane 3, PrP^c + 250x TNM; Lane 4; PrP^c + 1000x TNM; Lane 5, β-oligomer untreated control; Lane 6. β-oligomer + 250x PN; Lane 7. β-oligomer + 250x TNM.

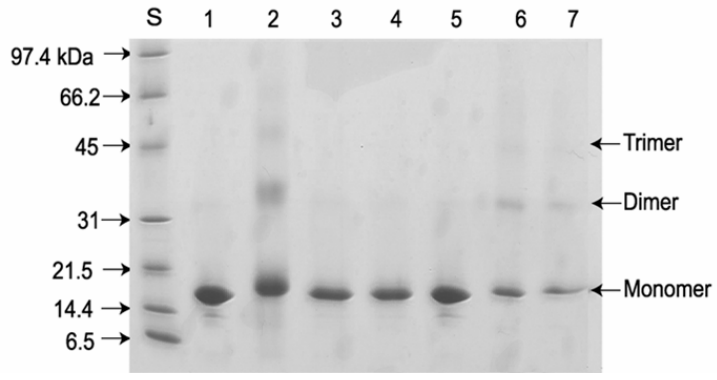

Using a higher concentration of TNM (1000x) increased the amount of nitro-Tyr formation in PrP^C to levels comparable to the 100x PN reactions. It is interesting that when PrP^C is treated with 1000x TNM, no evidence of crosslink formation or secondary structure changes was found, as judged by CD, AF_4, and SDS/PAGE techniques.

Trypsin, which cuts after Lys or Arg residues, produces six Tyr-containing peptides from PrP90 when digestion is followed by disulfide reduction. The tryptic peptide fragments from PrP90 conformers that were treated with either PN or TNM, or from untreated control samples, were analyzed by mass spectrometry. MALDI-TOF MS was used to determine which Tyr residues were labeled and the degree of nitration (Figure 4). Some methionine oxidation was also observed. For peptides containing nitro-Tyr, the expected MALDI-specific fragmentation pattern was observed; the nitroTyr peptide (+45) is partially degraded by the MALDI laser to produce fragments with masses corresponding to the loss of one or two oxygens (Figure 4, inset) (*56*). The signals for these masses were summed to provide the total nitration signal; the results for an average of three nitration reactions are summarized in Table 1. Except for the nitrated P5 peptide, which was difficult to detect by MALDI-TOF, the nitration levels of the Tyr-containing peptides were very consistent across the replicate reactions and digestions. Thus, the estimate of nitration for Y218 is more uncertain that for other Tyr residues.

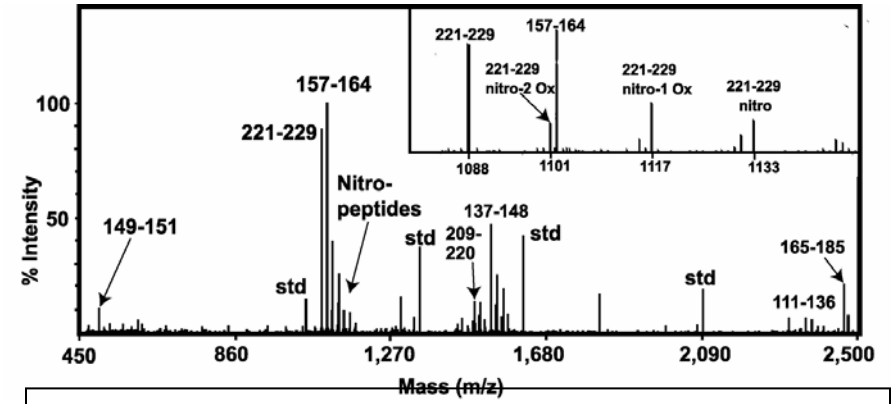

Figure 4. A partial MALDI-TOF spectrum of peptides from the tryptic digest of the β-oligomer, after reaction with 100x PN. Inset, expansion of the spectrum to show the loss of one or both oxygens from the nitro-group.

Patterns of Tyr Nitration in PrP^C

In cases where PN-labeled peptides contained more than one possible site of nitration, tandem mass spectrometry (ESI-MS/MS, Figure 5) was used to determine the site(s) of modification (Table 2). Since the tryptic peptide containing the first YYR motif ($Y_{149}Y_{150}R_{151}$) is small, aliquots of the nitrated protein were digested with cyanogen bromide to produce a larger peptide (peptide P2b, Table 2) containing this motif (*61*).

Peroxynitrite treatment of PrP^C results in the nitration of six Tyr residues. Y128, Y162, and Y163 were modified at low levels, Y218 at an intermediate level, and Y225 and Y226 at the highest levels (70 – 90%). Y162 and Y163 are part of the second YYR motif, and Y225 and Y226 are part of a conserved C-terminal YYD motif. No labeling was observed at Y149 or Y150 (the Tyr residues of the first YYR motif), Y157, or Y169. The average solvent accessible surface area was calculated using MOLMOL (*57*) for each Tyr residue, from the 25 best NMR solution structures found in PDB Accession #1B10 (*14*) (see Figure 6 for one structure). Y226 and Y225 are quite surface exposed and are the most readily nitrated. However, the relative reactivity of the other 8 Tyr residues does not correlate well with the degree of surface exposure.

y ion #	sequence	nitro-Y157	nitro-Y162	nitro-Y163
y(6)	$Y_{157}PNQVY_{162}Y_{169}R$	1147.53	1147.53	1147.53
y(7)	$PNQVY_{162}Y_{169}R$	939.49	984.49	984.49
y(6)	$NQVY_{162}Y_{169}R$	842.41	887.41	887.41
y(5)	$QVY_{162}Y_{169}R$	728.37	773.37	773.37
y(4)	$VY_{162}Y_{169}R$	600.31	645.31	645.31
y(3)	$Y_{162}Y_{169}R$	501.25	546.25	546.25
y(2)	$Y_{169}R$	338.18	338.18	338.18
y(1)	R	175.11	175.11	175.11

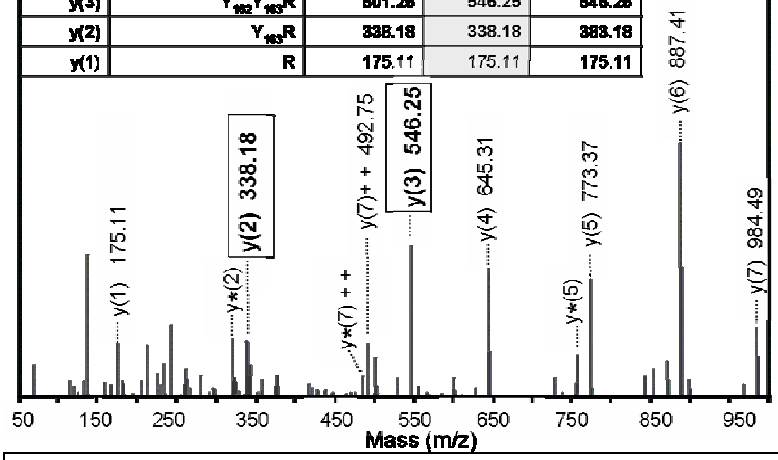

Figure 5. ESI-MS/MS spectrum of one mono-nitrated P3 peptide from the 100x PN/β-oligomer sample. Inset: the masses of the M+H y ions expected from each of the three potential sites of mono-nitration. (*) the loss of ammonia (-17) from R or Q; (++) doubly charged ions.

TNM, which nitrates by a different mechanism than PN (*62*), was much less reactive with PrP^C than PN; the only peptide that was found to be nitrated by 100x TNM was P6, which contains Y225 and Y226. When 1000x TNM was used to label PrP^C, higher levels of nitration were achieved. Analysis of the digested samples from 1000x TNM treatment showed that peptides P3 (Y157, Y162, Y163), P5 (Y218), and P6 (Y225, Y226) were labeled to a similar extent as when 100x PN was used. However, the higher concentration of TNM also labeled at P4 (Y169), which was not labeled by PN. Another difference between reagent reactivity was noted in P1 (Y128), which did not label with either concentration of TNM used but which was nitrated at low levels with PN.

As a whole, the data generated from both nitrating reagents show that in PrP^C, the most solvent exposed tyrosyl residues found in the C-terminal YYD are the most

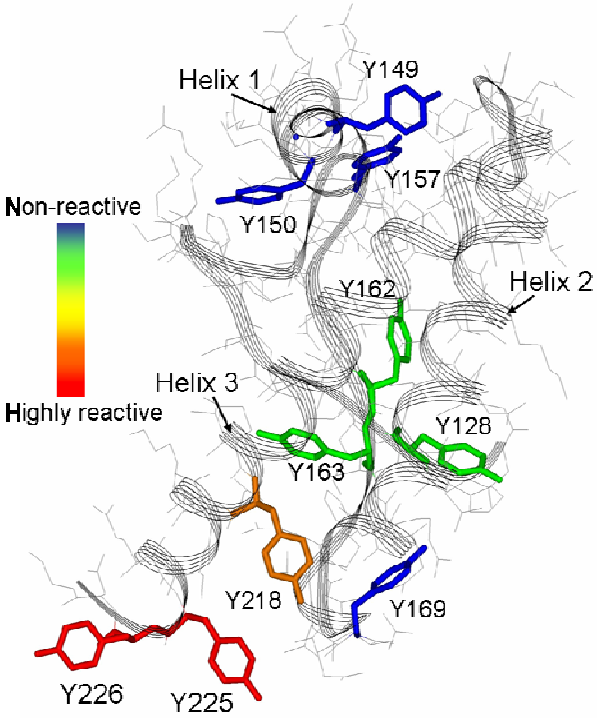

Figure 6. Structure of hamster PrP^C [14] indicating the locations and relative reactivities of the 10 Tyr residues after treatment with 100x PN.

reactive toward nitration. The first YYR motif (Y149-Y150-R151) is unreactive toward both reagents, whereas the second (Y162-Y163-R164) is labeled at low levels.

The thermal stabilities of untreated PrP^C and the products of its reaction with either 100x PN or 1000x TNM were measured by CD spectroscopy (Figure 7). The temperature at which 50% of untreated PrP^C is unfolded (T_m) was found to be 67 °C. This is higher than the T_m of 61.3 °C reported for the full length protein (*52*), which has a much larger unstructured N-terminal domain than the truncated PrP^C used in this study. Treatment of PrP^C with 1000x TNM did not affect the T_m, whereas the T_m decreased by 9°C for the 100x PN-treated sample. All samples show some deviation from simple two-state unfolding behavior (*63*) but the effect is more pronounced for the PN-treated sample. Deviation indicates that localized unfolding occurs in some parts of the protein, and/or that a portion of the total protein in the sample has fully unfolded at temperatures where most of the sample is intact.

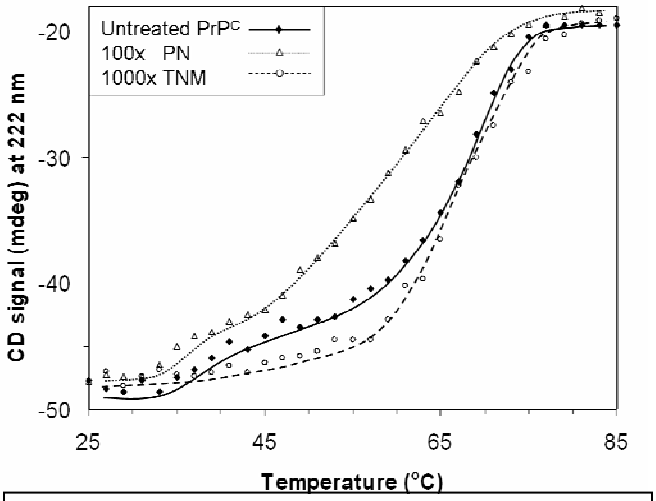

Figure 7. Thermal denaturation of PrP^c before and after treatment with 100x PN or 1000x TNM, as followed by the loss in CD signal at 222 nm (loss of α-helicity). (■) untreated PrP^c control (○) 100x PN reaction, (Δ) 1000x TNM reaction.

Patterns of Tyr Nitration in the β-Oligomer

When PN was used to label the β-oligomer, most Tyr residues that reacted in the PrP^C form were also found to be nitrated, although the reactivity of both Y225 and Y226 substantially decreased (Tables 1 and 2). The level of mono-nitration detected in peptide P3 (157-164) was similar in both PrP^C and the β-oligomer, and similar patterns of labeling were noted (no labeling at Y157, some labeling at Y163, majority of nitration at Y162). Two additional Tyr (Y149 and Y150) that are inert to nitration by PN in PrP^C are quite reactive in the β-oligomeric conformer. Tandem mass spectrometry showed that both of these residues, which are part of the first YYR motif, are capable of being nitrated, although nitro-Y149 was the dominant product detected. Identical nitration results were obtained for a sample of 250x PN-treated β-oligomer that had been separated from the cross-linked aggregates using the AF_4 methodology.

In stark contrast with the results obtained with PrP^C, TNM was an effective reagent for labeling the β-oligomer even at 100x concentration, and produced a similar pattern of nitro-Tyr formation as 100x PN. The only exception is Y128, which is labeled at low levels by PN in both PrP^C and β-oligomeric conformers but does not react with TNM in either conformation.

Discussion

Two nitrating reagents were used to probe for structural differences between PrP^C, the normal cellular form of prion protein, and the β-oligomeric conformer, which is closely related to the disease-associated conformation of PrP (*22-27*). Peroxynitrite (PN) is a water-soluble, powerful oxidant that uses a radical-based reaction mechanism to oxidize several amino acids, including Met, Cys (thiol form), Trp, and Tyr. In addition to the Tyr nitration discussed in this paper, some Met oxidation was also detected, but neither of the two Trp residues present in residues 90-232 of PrP was modified by PN (data not shown). The reactive form of PN is actually its protonated state, $HONO_2$, (pKa 6.8) (*64, 65*), which can oxidize amino acids directly in a bimolecular reaction, but has a half-life of only ~1 sec (*56*). $HONO_2$ decomposes to yield two radical species, hydroxide $OH^{\bullet}$ and nitrogen dioxide $NO_2^{\bullet}$. An intermediate reaction with CO_2 produces the carbonate radical $CO_3^{\bullet -}$ and $NO_2^{\bullet}$ (*65*). Any of these intermediate radicals are capable of oxidizing a Tyr residue to its radical state ($Tyr^{\bullet}$), which leads to the production of either nitro-Tyr or diTyr crosslinks.

The relative reactivity of a Tyr residue with PN is governed by its local protein environment (*66*). In approximate order of importance, these environmental factors that increase reactivity are (i) the lack of reactive Cys residues near the Tyr, (ii) the presence of a negatively charged residue, (iii) the absence of steric hindrance, (iv) surface (solvent) exposure, and (v) the presence of Tyr in a loop secondary structure. Of these, only (i) can be completely ruled out as influencing Tyr reactivity in PrP, since the only two Cys residues present in PrP are involved in disulfide bond formation in both isoforms studied here.

Tetranitromethane is soluble in organic solvents and so it is thought to more readily react with buried Tyr residues than PN. However, TNM has also been shown to nitrate surface Tyr residues (*67*). Its reactivity with Tyr residues is also governed by the protein microenvironment, which includes factors such as steric hindrance, hydrogen bonding to the Tyr hydroxyl group, and the presence of charged residues near the Tyr. It is proposed that Tyr residues with lower pKa values will be more reactive toward TNM, since the nitration mechanism involves formation of a tyrosinate/TNM charge transfer complex (*62*).

The observed patterns of Tyr nitration for PrP^C (Tables 1 and 2) support the premise that reactivity is influenced by more than one factor. The most readily nitrated Tyr residues (Y225,Y226) are clearly the most highly surface exposed residues. However, non-surface residues are also labeled to some degree. For these, no correlation with the presence of charged amino acids or hydrogen bonding was found. In fact, none of the identified factors that favor nitration are associated with Y218, yet this residue is quite susceptible to nitration in PrP^C. On the whole, the PrP^C data indicate that nitration should not be used to predict *global* protein structure, although it may serve as a good indicator of changes in local structure.

PrP^C was surprisingly stable toward TNM treatment. To achieve similar levels of nitration of PrP^C with TNM compared with 100x PN, a 1000-fold excess of reagent (100x

over Tyr) was required. Interestingly, the 1000x TNM-labeled PrP^C did not form any cross-linked products (Figure 3) as was noted for PN treatment. Moreover, the thermal denaturation profile (Figure 7), which is a measure of protein stability, was not modified for PrP^C treated with 1000x TNM compared with untreated PrP^C. In contrast, PN treatment of PrP^C destabilized the protein somewhat, as indicated by both the decrease in T_m and the rather large deviation from two-state unfolding behavior. This indicates that either there is some localized unfolding within the PN-treated sample, or that some population of the PN-treated PrP^C is completely unfolded at lower temperatures (is less stable) than the majority of the sample. Since these changes only occur for the 100x PN-treated sample and not for the 1000x TNM-treated sample, they cannot be attributed to the generic heterogeneity associated with a sample comprised of partially nitrated proteins. Rather, the destabilization of PrP^C by PN treatment is best explained by modifications of PrP^C that occur only when PN is used as the nitrating reagent. Of the ten Tyr residues, only Y128 is nitrated by PN but not by TNM. It is quite plausible that the nitration of Tyr128 would lead to protein instability. Tyr128 is adjacent to Met129 and is hydrogen bonded to Asp178 in many of the hamster PrP^C solution structures (*68*). Both Met129 and Asp178 are residues linked to human disease (*69-73*). The D178N polymorphism causes fatal familial insomnia if residue 129 is Met, and causes Creutzfeldt-Jakob disease if the variant Val129 is present. Moreover, the D178N mutation is predicted to eliminate the hydrogen bond between D178 and Y128, leading to the overall destabilization of the protein (*74, 75*). Thus, the protein destabilization noted in the thermal denaturation might be due to the presence of some nitro-Y128 protein in the ensemble of PN-treated PrP^C proteins. Increasing the PN concentration above 100x was associated with higher levels of nitro-Y128 formation (data not shown) and correlated with higher levels of protein unfolding and cross-linking (Figure 2A). Alternatively, the difference in protein stability between PrP^C treated with PN vs. TNM may arise from other oxidation events. We have noted that higher levels of Met oxidation occur when PN is the nitrating agent, and cannot rule out that oxidation of Met residues, in particular Met129, influences the overall protein stability, or that Met oxidation leads to the labeling of Y128.

The marked difference in TNM labeling of PrP^c vs the β-oligomer was surprising - only 100x TNM was required to nitrate ~30% of the Tyr residues and produce the same level of nitration as with 100x PN. The patterns of nitration are similar for the two reagents (Table 1), with the exception of Y128, which was again only susceptible to nitration by PN. Evidently formation of an oligomer does not prevent either reagent — the hydrophobic TNM or the water soluble PN — from accessing the susceptible Tyr residues. Interestingly, the two Tyr residues of the C-terminal YYD motif, Y225 and Y226, are ~50% less reactive toward both reagents. One of the published models for the fibrillar PrP^{Sc} state might account for this change. In the β-spiral model by Demarco and Daggett (*41*), Y225 and Y226 remain part of Helix 3, but the helix is near the subunit interface.

For both TNM and PN, the major difference in Tyr nitration between the two PrP isoforms occurs at Y149 and Y150. Y149 was labeled reasonably well and Y150 to a lesser degree by either PN or TNM in the β-oligomeric state, but neither residue was nitrated in the PrP^C isoform. Y159 and Y150 are part of the first conserved YYR motif.

Thus, our evidence strongly suggests that the first YYR motif, located on Helix 1 of PrP^{c}, undergoes a significant conformational change upon conversion to the β-oligomer. The data are consistent with these Tyr residues becoming more surface exposed in the β-oligomeric state, although other changes in the microenvironment might also influence the reactivity (*66*). The β-helix model (*39*) for PrP^{Sc} places both Y149 and Y150 in a surface exposed, solvent accessible environment, whereas in the β-spiral model (*41*), it is Y149 that undergoes a shift in surface exposure. Monoclonal antibody (MAb) work (*46-48*) supports the hypothesis that at least one of the YYR motifs becomes more surface accessible in PrP^{Sc}. In one study, anti-YYR antibodies were found to specifically recognize the diseased PrP^{Sc} conformation, which is structurally similar to the β-oligomer (*46*). These authors favor the second YYR motif as being the conformationally sensitive epitope. Other work using the PrP^{Sc}-specific MAb 15B3 (*47*) has identified a sequence containing the second YYR motif as part of its large, discontinuous epitope, but this MAb reportedly also recognizes the sequence immediately preceding the first YYR motif, so the results are not conclusive. A recent publication by Novitskaya et al (*48*) indicates that antibody AH6 (epitope159-174) binds to recombinant mouse PrP fibrils only after they are completely denatured by 6M guanidine-HCl. In contrast, antibody D18 (epitope 132-158) and IgG 136-158 are capable of binding under conditions where the fibrillar structure is still preserved, although neither bound in the absence of guanidine-HCl. Limited experiments were also conducted with the mouse β-oligomer, which also reacted with IgG 136-158 (D18 and AH6 were not tested).

The Tyr nitration results presented here provide an independent and complementary technique to antibody studies. The data clearly show that only the first YYR motif containing Y149 and Y150 is differentially nitrated by the two nitrating reagents PN and TNM. In contrast, the second YYR motif (Y162-Y163-R164) was nitrated only at low levels and in both conformers. This provides very strong evidence that upon conversion of PrP^{C} to the β-oligomer, the Helix 1 region containing the first YYR motif, residues 149 – 151, undergoes a large structural change. It is plausible that this change results in an increased surface exposure for these residues. Another change in local protein environment was noted for Y225 and Y226 in Helix 3, which showed a substantial decrease in nitration susceptibility in the β-oligomer. The similarities between the β-oligomer and the physiologically relevant PrP^{Sc} isoform suggest that these conformational changes are also of biological significance. Future experiments will examine the interactions of various MAbs with the nitrated PrP samples, and extend the nitration studies to include the recombinant fibrillar PrP and the PrP^{Sc} isoforms.

Acknowledgements

We thank Dr. Valerie Daggett and Dr. Cedric Govaerts for providing us with the PDB coordinates for their models, and Ms. Martha Rice for technical assistance.

References

(1) Priola, S. A., Chesebro, B., and Caughey, B. (2003) Biomedicine. A view from the top--prion diseases from 10,000 feet. *Science 300*, 917-9.

(2) Prusiner, S. B. (1998) Prions. *Proc Natl Acad Sci U S A 95*, 13363-83.

(3) Tan, S. Y., and Pepys, M. B. (1994) Amyloidosis. *Histopathology 25*, 403-14.

(4) Caughey, B., Raymond, G. J., Callahan, M. A., Wong, C., Baron, G. S., and Xiong, L. W. (2001) Interactions and conversions of prion protein isoforms. *Adv Protein Chem 57*, 139-69.

(5) Prusiner, S. B. (1982) Novel proteinaceous infectious particles cause scrapie. *Science 216*, 136-44.

(6) Caughey, B. W., Dong, A., Bhat, K. S., Ernst, D., Hayes, S. F., and Caughey, W. S. (1991) Secondary structure analysis of the scrapie-associated protein PrP 27-30 in water by infrared spectroscopy. *Biochemistry 30*, 7672-80.

(7) Stahl, N., Baldwin, M. A., Teplow, D. B., Hood, L., Gibson, B. W., Burlingame, A. L., and Prusiner, S. B. (1993) Structural studies of the scrapie prion protein using mass spectrometry and amino acid sequencing. *Biochemistry 32*, 1991-2002.

(8) Zahn, R., Liu, A., Luhrs, T., Riek, R., von Schroetter, C., Lopez Garcia, F., Billeter, M., Calzolai, L., Wider, G., and Wuthrich, K. (2000) NMR solution structure of the human prion protein. *Proc Natl Acad Sci U S A 97*, 145-50.

(9) Zahn, R., Guntert, P., von Schroetter, C., and Wuthrich, K. (2003) NMR structure of a variant human prion protein with two disulfide bridges. *J Mol Biol 326*, 225-34.

(10) Riek, R., Hornemann, S., Wider, G., Billeter, M., Glockshuber, R., and Wuthrich, K. (1996) NMR structure of the mouse prion protein domain PrP(121-321). *Nature 382*, 180-2.

(11) Lysek, D. A., Schorn, C., Nivon, L. G., Esteve-Moya, V., Christen, B., Calzolai, L., von Schroetter, C., Fiorito, F., Herrmann, T., Guntert, P., and Wuthrich, K. (2005) Prion protein NMR structures of cats, dogs, pigs, and sheep. *Proc Natl Acad Sci U S A 102*, 640-5.

(12) Lopez Garcia, F., Zahn, R., Riek, R., and Wuthrich, K. (2000) NMR structure of the bovine prion protein. *Proc Natl Acad Sci U S A 97*, 8334-9.

(13) Calzolai, L., Lysek, D. A., Perez, D. R., Guntert, P., and Wuthrich, K. (2005) Prion protein NMR structures of chickens, turtles, and frogs. *Proc Natl Acad Sci U S A 102*, 651-5.

(14) James, T. L., Liu, H., Ulyanov, N. B., Farr-Jones, S., Zhang, H., Donne, D. G., Kaneko, K., Groth, D., Mehlhorn, I., Prusiner, S. B., and Cohen, F. E. (1997) Solution structure of a 142-residue recombinant prion protein corresponding to the infectious fragment of the scrapie isoform. *Proc Natl Acad Sci U S A 94*, 10086-91.

(15) Gossert, A. D., Bonjour, S., Lysek, D. A., Fiorito, F., and Wuthrich, K. (2005) Prion protein NMR structures of elk and of mouse/elk hybrids. *Proc Natl Acad Sci U S A 102*, 646-50.

(16) Haire, L. F., Whyte, S. M., Vasisht, N., Gill, A. C., Verma, C., Dodson, E. J., Dodson, G. G., and Bayley, P. M. (2004) The crystal structure of the globular domain of sheep prion protein. *J Mol Biol 336*, 1175-83.

(17) Knaus, K. J., Morillas, M., Swietnicki, W., Malone, M., Surewicz, W. K., and Yee, V. C. (2001) Crystal structure of the human prion protein reveals a mechanism for oligomerization. *Nat Struct Biol 8*, 770-4.
(18) Eghiaian, F., Grosclaude, J., Lesceu, S., Debey, P., Doublet, B., Treguer, E., Rezaei, H., and Knossow, M. (2004) Insight into the PrPC-->PrPSc conversion from the structures of antibody-bound ovine prion scrapie-susceptibility variants. *Proc Natl Acad Sci U S A 101*, 10254-9.
(19) Wuthrich, K., and Riek, R. (2001) Three-dimensional structures of prion proteins. *Adv Protein Chem 57*, 55-82.
(20) Merz, P. A., Kascsak, R. J., Rubenstein, R., Carp, R. I., and Wisniewski, H. M. (1987) Antisera to scrapie-associated fibril protein and prion protein decorate scrapie-associated fibrils. *J Virol 61*, 42-9.
(21) Prusiner, S. B., McKinley, M. P., Bowman, K. A., Bolton, D. C., Bendheim, P. E., Groth, D. F., and Glenner, G. G. (1983) Scrapie prions aggregate to form amyloid-like birefringent rods. *Cell 35*, 349-58.
(22) Baskakov, I. V., Legname, G., Baldwin, M. A., Prusiner, S. B., and Cohen, F. E. (2002) Pathway complexity of prion protein assembly into amyloid. *J Biol Chem 277*, 21140-8.
(23) Tattum, M. H., Cohen-Krausz, S., Khalili-Shirazi, A., Jackson, G. S., Orlova, E. V., Collinge, J., Clarke, A. R., and Saibil, H. R. (2006) Elongated oligomers assemble into mammalian PrP amyloid fibrils. *J Mol Biol 357*, 975-85.
(24) Vendrely, C., Valadie, H., Bednarova, L., Cardin, L., Pasdeloup, M., Cappadoro, J., Bednar, J., Rinaudo, M., and Jamin, M. (2005) Assembly of the full-length recombinant mouse prion protein I. Formation of soluble oligomers. *Biochim Biophys Acta 1724*, 355-66.
(25) Zou, W. Q., and Cashman, N. R. (2002) Acidic pH and detergents enhance in vitro conversion of human brain PrPC to a PrPSc-like form. *J Biol Chem 277*, 43942-7.
(26) Leffers, K. W., Wille, H., Stohr, J., Junger, E., Prusiner, S. B., and Riesner, D. (2005) Assembly of natural and recombinant prion protein into fibrils. *Biol Chem 386*, 569-80.
(27) Novitskaya, V., Bocharova, O. V., Bronstein, I., and Baskakov, I. V. (2006) Amyloid fibrils of mammalian prion protein are highly toxic to cultured cells and primary neurons. *J Biol Chem 281*, 13828-36.
(28) Silveira, J. R., Raymond, G. J., Hughson, A. G., Race, R. E., Sim, V. L., Hayes, S. F., and Caughey, B. (2005) The most infectious prion protein particles. *Nature 437*, 257-61.
(29) Caughey, B. (2001) Interactions between prion protein isoforms: the kiss of death? *Trends Biochem Sci 26*, 235-42.
(30) Baskakov, I. V., Aagaard, C., Mehlhorn, I., Wille, H., Groth, D., Baldwin, M. A., Prusiner, S. B., and Cohen, F. E. (2000) Self-assembly of recombinant prion protein of 106 residues. *Biochemistry 39*, 2792-804.
(31) Flechsig, E., Shmerling, D., Hegyi, I., Raeber, A. J., Fischer, M., Cozzio, A., von Mering, C., Aguzzi, A., and Weissmann, C. (2000) Prion protein devoid of the octapeptide repeat region restores susceptibility to scrapie in PrP knockout mice. *Neuron 27*, 399-408.
(32) Supattapone, S., Muramoto, T., Legname, G., Mehlhorn, I., Cohen, F. E., DeArmond, S. J., Prusiner, S. B., and Scott, M. R. (2001) Identification of two prion protein regions that modify scrapie incubation time. *J Virol 75*, 1408-13.

(33) Fischer, M., Rulicke, T., Raeber, A., Sailer, A., Moser, M., Oesch, B., Brandner, S., Aguzzi, A., and Weissmann, C. (1996) Prion protein (PrP) with amino-proximal deletions restoring susceptibility of PrP knockout mice to scrapie. *Embo J 15*, 1255-64.
(34) Frankenfield, K. N., Powers, E. T., and Kelly, J. W. (2005) Influence of the N-terminal domain on the aggregation properties of the prion protein. *Protein Sci 14*, 2154-66.
(35) Lawson, V. A., Priola, S. A., Wehrly, K., and Chesebro, B. (2001) N-terminal truncation of prion protein affects both formation and conformation of abnormal protease-resistant prion protein generated in vitro. *J Biol Chem 276*, 35265-71.
(36) Lawson, V. A., Priola, S. A., Meade-White, K., Lawson, M., and Chesebro, B. (2004) Flexible N-terminal region of prion protein influences conformation of protease-resistant prion protein isoforms associated with cross-species scrapie infection in vivo and in vitro. *J Biol Chem 279*, 13689-95.
(37) Pan, K. M., Baldwin, M., Nguyen, J., Gasset, M., Serban, A., Groth, D., Mehlhorn, I., Huang, Z., Fletterick, R. J., Cohen, F. E., and et al. (1993) Conversion of alpha-helices into beta-sheets features in the formation of the scrapie prion proteins. *Proc Natl Acad Sci U S A 90*, 10962-6.
(38) Wille, H., Michelitsch, M. D., Guenebaut, V., Supattapone, S., Serban, A., Cohen, F. E., Agard, D. A., and Prusiner, S. B. (2002) Structural studies of the scrapie prion protein by electron crystallography. *Proc Natl Acad Sci U S A 99*, 3563-8.
(39) Govaerts, C., Wille, H., Prusiner, S. B., and Cohen, F. E. (2004) Evidence for assembly of prions with left-handed beta-helices into trimers. *Proc Natl Acad Sci U S A 101*, 8342-7.
(40) Anderson, M., Bocharova, O. V., Makarava, N., Breydo, L., Salnikov, V. V., and Baskakov, I. V. (2006) Polymorphism and ultrastructural organization of prion protein amyloid fibrils: an insight from high resolution atomic force microscopy. *J Mol Biol 358*, 580-96.
(41) DeMarco, M. L., and Daggett, V. (2004) From conversion to aggregation: protofibril formation of the prion protein. *Proc Natl Acad Sci U S A 101*, 2293-8.
(42) Malolepsza, E., Boniecki, M., Kolinski, A., and Piela, L. (2005) Theoretical model of prion propagation: a misfolded protein induces misfolding. *Proc Natl Acad Sci U S A 102*, 7835-40.
(43) Langedijk, J. P., Fuentes, G., Boshuizen, R., and Bonvin, A. M. (2006) Two-rung Model of a Left-handed beta-Helix for Prions Explains Species Barrier and Strain Variation in Transmissible Spongiform Encephalopathies. *J Mol Biol*.
(44) Yang, S., Levine, H., Onuchic, J. N., and Cox, D. L. (2005) Structure of infectious prions: stabilization by domain swapping. *Faseb J 19*, 1778-82.
(45) Cox, D. L., Pan, J., and Singh, R. R. (2006) A mechanism for copper inhibition of infectious prion conversion. *Biophys J*.
(46) Paramithiotis, E., Pinard, M., Lawton, T., LaBoissiere, S., Leathers, V. L., Zou, W. Q., Estey, L. A., Lamontagne, J., Lehto, M. T., Kondejewski, L. H., Francoeur, G. P., Papadopoulos, M., Haghighat, A., Spatz, S. J., Head, M., Will, R., Ironside, J., O'Rourke, K., Tonelli, Q., Ledebur, H. C., Chakrabartty, A., and Cashman, N. R. (2003) A prion protein epitope selective for the pathologically misfolded conformation. *Nat Med 9*, 893-9.
(47) Korth, C., Stierli, B., Streit, P., Moser, M., Schaller, O., Fischer, R., Schulz-Schaeffer, W., Kretzschmar, H., Raeber, A., Braun, U., Ehrensperger, F., Hornemann, S.,

Glockshuber, R., Riek, R., Billeter, M., Wuthrich, K., and Oesch, B. (1997) Prion (PrPSc)-specific epitope defined by a monoclonal antibody. *Nature 390*, 74-7.

(48) Novitskaya, V., Makarava, N., Bellon, A., Bocharova, O. V., Bronstein, I. B., Williamson, R. A., and Baskakov, I. V. (2006) Probing the conformation of the prion protein within a single amyloid fibril using a novel immunoconformational assay. *J Biol Chem 281*, 15536-45.

(49) Moroncini, G., Mangieri, M., Morbin, M., Mazzoleni, G., Ghetti, B., Gabrielli, A., Williamson, R. A., Giaccone, G., and Tagliavini, F. (2006) Pathologic prion protein is specifically recognized in situ by a novel PrP conformational antibody. *Neurobiol Dis*.

(50) Turko, I. V., and Murad, F. (2005) Mapping sites of tyrosine nitration by matrix-assisted laser desorption/ionization mass spectrometry. *Methods Enzymol 396*, 266-75.

(51) Wong, P. S., and van der Vliet, A. (2002) Quantitation and localization of tyrosine nitration in proteins. *Methods Enzymol 359*, 399-410.

(52) Speare, J. O., Rush, T. S., 3rd, Bloom, M. E., and Caughey, B. (2003) The role of helix 1 aspartates and salt bridges in the stability and conversion of prion protein. *J Biol Chem 278*, 12522-9.

(53) Sambrook, J., and Russell, D. W. (2001) *Molecular Cloning, A Laboratory Manual*, Third ed., Cold Spring Harbor Laboratory Press, New York.

(54) Pace, C. N., Vajdos, F., Fee, L., Grimsley, G., and Gray, T. (1995) How to measure and predict the molar absorption coefficient of a protein. *Protein Sci 11*, 2411-2423.

(55) King, P. A., Jamison, E., Strahs, D., Anderson, V. E., and Brenowitz, M. (1993) 'Footprinting' proteins on DNA with peroxonitrous acid. *Nucleic Acids Res 21*, 2473-8.

(56) Sarver, A., Scheffler, N. K., Shetlar, M. D., and Gibson, B. W. (2001) Analysis of peptides and proteins containing nitrotyrosine by matrix-assisted laser desorption/ionization mass spectrometry. *J Am Soc Mass Spectrom 12*, 439-48.

(57) Koradi, R., Billeter, M., and Wuthrich, K. (1996) MOLMOL: a program for display and analysis of macromolecular structures. *J Mol Graph 14*, 51-5, 29-32.

(58) Sokolowski, F., Modler, A. J., Masuch, R., Zirwer, D., Baier, M., Lutsch, G., Moss, D. A., Gast, K., and Naumann, D. (2003) Formation of critical oligomers is a key event during conformational transition of recombinant syrian hamster prion protein. *J Biol Chem 278*, 40481-92.

(59) Rezaei, H., Eghiaian, F., Perez, J., Doublet, B., Choiset, Y., Haertle, T., and Grosclaude, J. (2005) Sequential generation of two structurally distinct ovine prion protein soluble oligomers displaying different biochemical reactivities. *J Mol Biol 347*, 665-79.

(60) Hirel, P. H., Schmitter, M. J., Dessen, P., Fayat, G., and Blanquet, S. (1989) Extent of N-terminal methionine excision from Escherichia coli proteins is governed by the side-chain length of the penultimate amino acid. *Proc Natl Acad Sci U S A 86*, 8247-51.

(61) Lee, T. D., and Shively, J. E. (1990) Enzymatic and chemical digestion of proteins for mass spectrometry. *Methods Enzymol 193*, 361-74.

(62) Bruice, T. C., Gregory, M. J., and Walters, S. L. (1968) Reactions of tetranitromethane. I. Kinetics and mechanism of nitration of phenols by tetranitromethane. *J.Amer.Chem.Soc. 90*, 1612.

(63) Eftink, M. R. (1995) Use of multiple spectroscopic methods to monitor equilibrium unfolding of proteins. *Methods Enzymol 259*, 487-512.

(64) Batthyany, C., Souza, J. M., Duran, R., Cassina, A., Cervenansky, C., and Radi, R. (2005) Time course and site(s) of cytochrome c tyrosine nitration by peroxynitrite. *Biochemistry 44*, 8038-46.
(65) Radi, R., Cassina, A., Hodara, R., Quijano, C., and Castro, L. (2002) Peroxynitrite reactions and formation in mitochondria. *Free Radic Biol Med 33*, 1451-64.
(66) Souza, J. M., Daikhin, E., Yudkoff, M., Raman, C. S., and Ischiropoulos, H. (1999) Factors determining the selectivity of protein tyrosine nitration. *Arch Biochem Biophys 371*, 169-78.
(67) Petersson, A. S., Steen, H., Kalume, D. E., Caidahl, K., and Roepstorff, P. (2001) Investigation of tyrosine nitration in proteins by mass spectrometry. *J Mass Spectrom 36*, 616-25.
(68) Liu, H., Farr-Jones, S., Ulyanov, N. B., Llinas, M., Marqusee, S., Groth, D., Cohen, F. E., Prusiner, S. B., and James, T. L. (1999) Solution structure of Syrian hamster prion protein rPrP(90-231). *Biochemistry 38*, 5362-77.
(69) Apetri, A. C., Vanik, D. L., and Surewicz, W. K. (2005) Polymorphism at residue 129 modulates the conformational conversion of the D178N variant of human prion protein 90-231. *Biochemistry 44*, 15880-8.
(70) Baskakov, I., Disterer, P., Breydo, L., Shaw, M., Gill, A., James, W., and Tahiri-Alaoui, A. (2005) The presence of valine at residue 129 in human prion protein accelerates amyloid formation. *FEBS Lett 579*, 2589-96.
(71) Gambetti, P. (1996) Fatal familial insomnia and familial Creutzfeldt-Jakob disease: a tale of two diseases with the same genetic mutation. *Curr Top Microbiol Immunol 207*, 19-25.
(72) Zarranz, J. J., Digon, A., Atares, B., Rodriguez-Martinez, A. B., Arce, A., Carrera, N., Fernandez-Manchola, I., Fernandez-Martinez, M., Fernandez-Maiztegui, C., Forcadas, I., Galdos, L., Gomez-Esteban, J. C., Ibanez, A., Lezcano, E., Lopez de Munain, A., Marti-Masso, J. F., Mendibe, M. M., Urtasun, M., Uterga, J. M., Saracibar, N., Velasco, F., and de Pancorbo, M. M. (2005) Phenotypic variability in familial prion diseases due to the D178N mutation. *J Neurol Neurosurg Psychiatry 76*, 1491-6.
(73) Gambetti, P., Parchi, P., and Chen, S. G. (2003) Hereditary Creutzfeldt-Jakob disease and fatal familial insomnia. *Clin Lab Med 23*, 43-64.
(74) Barducci, A., Chelli, R., Procacci, P., Schettino, V., Gervasio, F. L., and Parrinello, M. (2006) Metadynamics simulation of prion protein: beta-structure stability and the early stages of misfolding. *J Am Chem Soc 128*, 2705-10.
(75) Gsponer, J., Ferrara, P., and Caflisch, A. (2001) Flexibility of the murine prion protein and its Asp178Asn mutant investigated by molecular dynamics simulations. *J Mol Graph Model 20*, 169-82.

Table 1. MALDI/TOF analysis of Tyr-containing PrP peptides produced by trypsin digestion. The Solvent Accessible Surface Area (SASA) shown is the average value for all NMR solution structures from PDB #1B10, using the program MOLMOL. Nitration Key: **-**, 0 to 5% nitration; **+**, 6 to 20% nitration; **++**, 21 to 45% nitration; **+++**, 46-70%, **++++**, 71 to 100% nitration.

Tryptic Peptide Sequence (% SASA)		**100x PN PrP^C**	**100x TNM PrP^C**	**1000x TNM PrP^C**	**100x PN β-oligomer**	**100x TNM β-oligomer**
P1 (residues 111-136) HMAGAAAAGAVVGGLGG**Y_{128}**MLGSAMSR (Y128, 5.6%)		**+**	**-**	**-**	**+**	**-**
P2a (residues 149-151) **$Y_{149}Y_{150}$**R (Y149, 13.7%; Y150, 2.8%)	Mono-nitration	**-**	**-**	**-**	**+++**	**+++**
	Di-nitration	**-**	**-**	**-**	**-**	**-**
P3 (residues 157-164) **Y_{157}**PNQV**$Y_{162}Y_{163}$**R (Y157, 2%; Y162, 11.7%; Y163, 3.3%)	Mono-nitration	**+**	**-**	**+**	**+**	**++**
	Di-nitration	**-**	**-**	**-**	**-**	**-**
	Tri-nitration	**-**	**-**	**-**	**-**	**-**
P4 (residues 165-185) PVDQ**Y_{169}**NNQNNFVHDCVNITIK (Y169, 16.4%)		**-**	**-**	**++**	**+**	**+**
P5 (residues 209-220) VVEQMCTTQ**Y_{218}**QK (Y218, 5.6%)		**+++**	**-**	**+++**	**++**	**++**
P6 (residues 221-229) ESQA**$Y_{225}Y_{226}$**DGR (Y225, 39%; Y226, 59%)	Mono-nitration	**++++**	**+**	**++++**	**++**	**++**
	Di-nitration	**++**	**-**	**++**	**-**	**-**

Table 2. ES-MS/MS sequencing results for mono-nitrated peroxynitrite-labeled peptides that contain more than one potential site of nitration. The number of ions detected for each nitrated product is indicated for each sample.

Peptide Sequence	**100x PN PrP^C**		**100x PN β-oligomer**	
P2b (residues 140-154) HFGNDWEDR**$Y_{149}$$Y_{150}$**RENM	None Detected		Nitro-Y_{149} Nitro-Y_{150}	3 1
P3 (residues 157-164) **Y_{157}**PNQV**$Y_{162}$$Y_{163}$**R	Nitro-Y_{157} Nitro-Y_{162} Nitro-Y_{163}	0 11 5	Nitro-Y_{157} Nitro-Y_{162} Nitro-Y_{163}	0 4 1
P6 (residues 221-229) ESQA**$Y_{225}$$Y_{226}$**DGR	Nitro-Y_{225} Nitro-Y_{226}	2 7	Nitro-Y_{225} Nitro-Y_{226}	2 2

Figure Legends:

Figure 1. CD spectra of PrP conformational isomers. Inset: the AF_4 elution profiles (detection at 280 nm) showing the time course of the chemical conversion of PrP^c to the β-oligomer. Times of conversion: t = 0, 15s, 30s, 30 min, and 160 min.

Figure 2. AF_4 elution profiles of the PrP isoforms treated with increasing concentrations of PN. (——) untreated control, (**-----**) 100x PN reaction, (·····) 250x PN reaction. (**A**) the PrP^C isoform, with the corresponding CD spectra presented (inset). (**B**) the β-oligomer.

Figure 3. SDS/PAGE analysis of PN and TNM reactions with PrP^C and the β-oligomer. Lane S, MW standard;. Lane 1, PrP^c untreated control; Lane 2, PrP^c + 250x PN; Lane 3, PrP^c + 250x TNM; Lane 4; PrP^c + 1000x TNM; Lane 5, β-oligomer untreated control; Lane 6. β-oligomer + 250x PN; Lane 7. β-oligomer + 250x TNM.

Figure 4. A partial MALDI-TOF spectrum of peptides from the tryptic digest of the β-oligomer, after reaction with 100x PN. Inset, expansion of the spectrum to show the loss of one or both oxygens from the nitro-group.

Figure 5. ESI-MS/MS spectrum of one mono-nitrated P3 peptide from the 100x PN/β-oligomer sample. Inset: the masses of the M+H y ions expected from each of the three potential sites of mono-nitration. (*) the loss of ammonia (-17) from R or Q; (++) doubly charged ions.

Figure 6. Structure of hamster $PrP^{C\ 14}$ indicating the locations and relative reactivities of the 10 Tyr residues after treatment with 100x PN.

Figure 7. Thermal denaturation of PrP^c before and after treatment with 100x PN or 1000x TNM, as followed by the loss in CD signal at 222 nm (loss of α-helicity). (■) untreated PrP^c control (○) 100x PN reaction, (Δ) 1000x TNM reaction.